Research Article | Vol. 27, No. 21 / 14 October 2019 / Optics Express 30681
Optics EXPRESS

Single-cycle scalable terahertz pulse source in reflection geometry

GYÖRGY TÓTH,[1,*] LÁSZLÓ PÁLFALVI,[1] ZOLTÁN TIBAI,[1] LEVENTE TOKODI,[1] JÓZSEF A. FÜLÖP,[2,3] ZSUZSANNA MÁRTON,[1] GÁBOR ALMÁSI,[1,3] AND JÁNOS HEBLING[1,2,3]

[1]*Institute of Physics, University of Pécs, 7624 Pécs, Hungary*
[2]*Szentágothai Research Centre, University of Pécs, 7624 Pécs, Hungary*
[3]*MTA-PTE High-Field Terahertz Research Group, 7624 Pécs, Hungary*
[*]*tothgy@fizika.ttk.pte.hu*

Abstract: A tilted-pulse-front pumped terahertz pulse source is proposed for the generation of extremely high field single-cycle terahertz pulses. The very simple and compact source consists of a single crystal slab having a blazed reflection grating grooved in its back surface. Its further important advantages are the energy scalability and the symmetric THz beam profile. Generation of ~50 MV/cm focused field with 10.8 mJ terahertz pulse energy is predicted for a 7 cm diameter $LiNbO_3$ crystal, if the pump pulse is of 870 mJ energy, 1030 nm central wavelength and 1 ps pulse duration. Such sources can decisively promote the realization of THz driven electron and proton accelerators and open the way for a new generation concept of terahertz pulses having extreme high field.

1. Introduction

Acceleration of electrons [1,2] and protons [3,4] are promising applications of THz pulses with extremely high (> 100 kV/cm) electric field. Optical rectification of ultrashort laser pulses in nonlinear materials (NMs) can be appropriate for efficient generation of such THz pulses. The highest so far THz pulse energy (0.9 mJ) was achieved by using the organic DSTMS as NM [5]. However, the spectrum obtained from organic materials is typically centered in the 2 to 10 THz, while lower frequencies are more suitable for particle acceleration. The frequency range below 2 THz can be better accessed with lithium niobate ($LiNbO_3$, abbreviated as LN in the followings), utilizing the tilted-pulse-front (TPF) technique for non-collinear phase matching [6]. Presently, THz pulse energy in the mJ level is available with TPF excited THz sources using LN [7].

In the TPF excitation geometry, the velocity matching reads as

$$v_{p,gr}\cos(\gamma) = v_{THz,ph}, \tag{1}$$

where $v_{p,gr}$ is the group velocity of the pump pulse, $v_{THz,ph}$ is the phase velocity of the THz pulse, and γ is the pulse-front-tilt angle, which is ~63° for LN.

LN based TPF sources have been demonstrated to be very effective and, because of this, are widely applied in THz pump-probe experiments supporting few μJ THz pulses. However, the large necessary tilt-angle and the correspondingly large angular dispersion of the pump beam bring about three types of strong limitations. These are the following: (i) Imaging errors in the presence of angular dispersion result in a lengthened pulse duration at the edges of the pump spot [8,9]. (ii) In order to enable perpendicular incoupling of the pump and perpendicular outcoupling of the THz beam, a prism-shaped nonlinear crystal has to be used with a wedge angle equal to the tilt angle γ. This results in THz pulses with different temporal shapes at the edges of the THz beam because of the different generation lengths. Such a bad quality, strongly asymmetric THz beam drastically hinders many applications, especially particle acceleration. (iii) Due to the large group-delay-dispersion (GDD) associated to the angular dispersion [10], an ultrashort

#372207 https://doi.org/10.1364/OE.27.030681
Journal © 2019 Received 9 Jul 2019; revised 21 Aug 2019; accepted 21 Aug 2019; published 9 Oct 2019

Optics EXPRESS

pump pulse evolves very fast inside the LN crystal, and the average pulse duration becomes much longer than the Fourier transform-limited (FL) pump pulse duration.

Problems (i) and (ii) can be eliminated, in principle, using contact-grating set-ups [11]. An efficient contact-grating set-up was realized using ZnTe semiconductor as NM [12]. Contact grating setups were designed and realized for LN, too [13,14]. However, because of technical difficulties induced by the large needed tilt angle, efficient generation of THz pulses has failed yet.

In order to mitigate problem (iii) one should use a semiconductor crystal, which requires lower pulse-front-tilt, or longer FL pump pulse duration can be applied [8]. As another solution, the effect of the angular dispersion can be avoided by using a stair-step echelon structure. In this case a stair-step shaped, segmented tilted-pulse-front is formed instead of a continuous one. The first suggestion and demonstration of such a source type was published in [15]. Efficient generation of THz pulses by 70 fs long pump pulses were demonstrated by using a reflective echelon [15]. Disadvantageously, however, this echelon setup also requires both imaging and a prism-shaped NM with the same large γ wedge angle as the conventional setup.

Recently we suggested a so called "nonlinear echelon slab" (NLES) THz source, which is a NM with an echelon-like profile created on its entrance surface. This configuration has the advantage that a slab-like NM can be used, and that it also reduces the imaging errors. High THz conversion efficiency with symmetric, homogeneous THz beam can be achieved if appropriate pre-tilt is applied in the pump beam [16,17]. Although the slab-like structure allows significant energy scalability, imaging errors still remain a limiting factor. Simulations for a modified NLES setup predicts good THz conversion efficiency in an imaging free configuration as well [18]. Disadvantageously, it is necessary that the NLES has a small wedge angle.

In the present paper, we propose a very simple, compact, energy-scalable THz pulse source that avoids limiting factors (i) and (ii), and in special implementation even limiting factor (iii). The key feature of the new design is, that a blazed reflective grating structure is created on the backside of a nonlinear slab. High diffraction efficiency can be achieved with this structure using a course grating in high diffraction order. Neither a pre-tilt of the pump beam, nor imaging optics have to be used. High THz energies with excellent THz beam properties are predicted with this simple and compact setup.

2. RNLS THz source

The presently proposed THz source consists of only the pump source and a reflective nonlinear slab (RNLS). Here we emphasize, that this compactness is a very important advantage of the setup. Figure 1 depicts the RNLS itself. It is made from a plan parallel nonlinear crystal slab (LN is supposed). The front (top) surface of the slab remains plane, but in its back (bottom) surface a periodic structure is created (e.g. by diamond milling [19]) in order to form a blazed reflective grating. According to the geometry of the grating structure, we distinguish two different implementations (symmetric and asymmetric ones). We focus on the symmetric one in the present paper. The asymmetric version might also have relevance, but we do not discuss it here.

The pump beam incident perpendicular to the top surface of the slab (see Fig. 1) does not generate practically any THz radiation when it propagates inside the NM towards the back surface, since velocity matching condition is not fulfilled. The diffraction of the pump beam arriving perpendicular to the back surface are determined by the

$$\sin(\beta_m) = \mathrm{m}\frac{\lambda}{d \cdot n_p} \tag{2}$$

grating equation, where d is the period of the structure on the back surface (the blazed grating), n_p is the phase refractive index of the NM at the pump wavelength, and β_m is the diffraction angle of the beam belonging to the m^{th} diffraction order. The ± orders are arranged symmetrically to

Optics EXPRESS

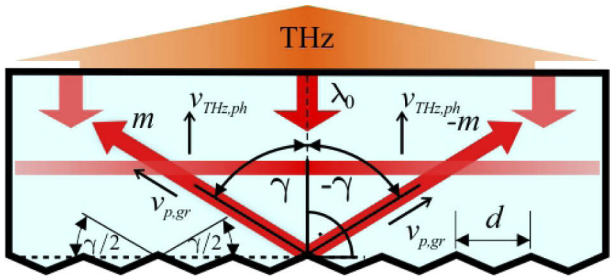

Fig. 1. A schematic figure of the reflective nonlinear slab (RNLS) THz source. The red color concerns the pump.

the normal of the grating (similarly as in the contact grating scheme examined in [12,20]). Since the grating structure is symmetric, the beams of the +m and -m orders have the same intensity. The diffraction introduces the needed tilt of the tangential plane of the intensity fronts of the $\pm m^{th}$ order beam if $\beta_m = \gamma$ and $\beta_{-m} = -\gamma$. This can be achieved by adequate choice of the m/d ratio. In the $+m^{th}$ and $-m^{th}$ order, the tilted fronts of the beams overlap each other (the red line in Fig. 1) and are parallel to the front surface, and the velocity component in the direction of the normal of the grating is $v_{p,gr}\cos(\gamma) = v_{THz,ph}$, satisfying the velocity matching condition. The generated THz pulse propagates perpendicularly to the tilted-pulse-front i.e. also perpendicularly to the front surface of the RNLS. Hence, the THz beam exits from the slab without deflection.

In order to obtain large diffraction efficiency, the grating has to be blazed with blaze angle equal to $\gamma/2$. It was shown by COMSOL simulations, that for course grating high diffraction efficiency can be achieved in a chosen diffraction order. The diffraction efficiency of the ±m diffraction order together with the necessary grating constant achieving $\beta_m = \gamma$ can be seen in Fig. 2(a) for 800 and 1030 nm pump wavelengths. We have examined the diffraction efficiency for two cases, namely for gold reflection coating on the back side of the RNLS (LN-Au) and in the absence of any coating (LN-Air), since both solutions might have practical relevance. However,

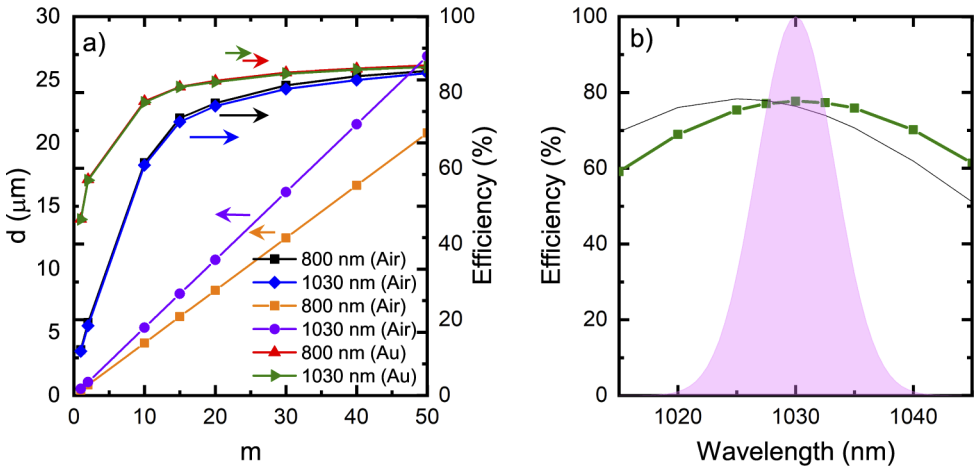

Fig. 2. (a)Diffraction efficiency and grating period versus the diffraction order for 800 and 1030 nm wavelengths.(b) The wavelength dependence of the diffraction efficiency for the m = 20 diffraction order and blazing angle of $\gamma/2 = 31.7°$ (black line) and 32.0° (green line), respectively. For reference the spectrum of a 200 fs FL pump pulse is also shown.

Optics EXPRESS

the gold coating can decrease the damage threshold of the structure. Thus our simulations were restricted to LN-air boundary within the frame of this preliminary work.

It is seen in Fig. 2. that the efficiency approaches the ~80% saturation value for m > 20. We supposed m = 20 in the calculations . In order to have information on the diffraction efficiency for broadband pump pulses, Fig. 2(b) shows the wavelength dependence of the diffraction efficiency for the m = 20 diffraction order as an example. As it is shown, for $\gamma/2$ blaze angle the wavelength dependent efficiency is not symmetric around the central wavelength of the pump. In order to achieve the advantageous symmetric efficiency dependence, the blaze angle was slightly changed. For example, using 1030 nm central pump wavelength at room temperature, the efficiency becomes symmetrical around the central wavelength if the blaze angle is 32.0° instead of $\gamma/2 = 31.7°$ (see Fig. 2(b)).

Since there is spatial overlap between the incident pump and the outcoming THz beams, they have to be separated. It can be done by applying a dichroic beam splitter (e.g. InO_2), or by slightly tilting out the slab from the orientation perpendicular to the propagation direction of the incoming pump.

3. Numerical model

A simple model was developed in order to obtain quantitative information on the optical-to-THz conversion efficiency and on the THz pulse shape and spectra for the reflective slab source introduced in Section 2. The model described in [16] for THz generation by optical rectification was adapted to the proposed new setup. The noncollinear excitation geometry, as well as the variation of the pump pulse length with the propagation due to the material and angular dispersion were taken into consideration in the model.

Let us suppose a Gaussian initial temporal shape of the optical pump pulse: $E(t) = \mathrm{Re}\left[E_0 \exp\left(-2\ln(2)\, t^2/\tau_0^2\right) \exp\left(i\omega_0 t\right)\right]$, where E_0 is the peak electric field-strength and τ_0 is the FL pump pulse length (FWHM). Taking into account the nonlinear polarization in the same way as in [21], the differential equation for the $E_{THz}(\Omega, z')$ Fourier component of the THz field reads as:

$$\begin{aligned}&\frac{\partial}{\partial z'} E_{THz}(\Omega, z') = \\ &-i\frac{\Omega d_{eff} E_0^2 \tau_0}{4\sqrt{\pi\ln(2)}\, c\, n_{THz,ph}(\omega)} \exp\left[-\frac{\left(\tau_0^2 + \Delta\tau(z')^2\right)\Omega^2}{16\ln(2)}\right] \times \\ &\exp\left[i\frac{\Omega}{c}\left(n_{THz,ph}(\Omega) - \frac{n_{p,gr}}{\cos(\gamma)}\right) z'\right] - \frac{\alpha_{THz}(\Omega)}{2} E_{THz}(\Omega, z'),\end{aligned} \tag{3}$$

where z' is the THz propagation coordinate, c is the speed of light in vacuum, Ω is the angular frequency of the THz radiation, $n_{THz,ph} = c/v_{THz,ph}$ is the THz phase index of refraction, $\alpha_{THz}(\Omega)$ is the THz (intensity) absorption coefficient, d_{eff} is the effective nonlinear coefficient (d_{eff} = 168 pm/V for LN), and $n_{p,gr}$ is the group refractive index of the pump. The relation between the z' THz propagation coordinate and the z_p pump coordinate is

$$z' = z_p \cos(\gamma). \tag{4}$$

One way to increase the effective interaction length (defined in [8]) is to compensate for the effects of material and angular dispersion (see the first exponential term of Eq. (3)) by pre-chirping the pulses [8,20]. In this way, one can set the pump-pulse length to be minimal (i.e., equal to the FL value) not at the entrance, but inside the crystal by tuning the pre-chirp. Instead of following the complex optimization procedure given in [20], we set the FL pulse length value simply at the crystal center (at $z' = L/2$, where L is the thickness of the slab) [8].

In Eq. (3), $\Delta\tau(z')$ is the delay between the short and long wavelength components at the half of the spectral intensity maximum of the pump pulse at z'. Starting from the dispersion parameter,

Optics EXPRESS

for the case of simultaneous presence of angular and material dispersion [10], one can obtain

$$\Delta\tau(z') = \frac{\lambda_0}{c}\frac{z' - L/2}{\cos(\gamma)}\left(\frac{n_{p,gr}^2}{n_p}\frac{\tan^2(\gamma)}{\lambda_0^2} - \frac{\mathrm{d}^2 n_p}{\mathrm{d}\lambda^2}\right)\Delta\lambda, \tag{5}$$

where $\Delta\lambda$ is the spectral bandwidth (FWHM). As can be seen $\Delta\tau(L/2) = 0$ meaning that the FL pump pulse length is obtained at the middle of the crystal as it was aimed.

The second exponential factor in Eq. (3) takes into account any remaining velocity mismatch coming from the effect of the dispersion in the THz range. Terahertz absorption, which is taken into account in the very last term of Eq. (3), is related only to the lattice. Absorption by free-carriers, generated by multiphoton absorption is neglected. Any nonlinear effects (except the optical rectification), such as pump depletion, and self-phase modulation were also neglected.

The THz fluence at the output can be determined from the solution of Eq. (3) as

$$Fluence_{THz} = \frac{\epsilon_0 c}{2} 2\pi \int_0^\infty \left| E_{THz}(\Omega, L)\frac{2n_{THz,ph}}{n_{THz,ph} + 1}\right|^2 \mathrm{d}\Omega. \tag{6}$$

Fresnel reflections, which cause a significant loss, are also accounted for by this formula. The pump fluence is:

$$Fluence_p = \sqrt{\frac{\pi}{2}}\frac{\epsilon_0 n_p}{2}E_0^2\frac{\tau_0}{\sqrt{2\ln(2)}} \tag{7}$$

and the optical-to-THz conversion efficiency is:

$$\eta = \frac{Fluence_{THz}}{Fluence_p}\eta_D, \tag{8}$$

where η_D is the diffraction efficiency of the reflection grating (see Fig. 2).

A 0.68 mol% doped stoichiometric LN was supposed as NM, and the temperature was supposed to be 300 K in the simulations. Two widely used laser types were assumed as pumping sources, which differ not only in their central wavelength but also in the typical pulse lengths. One of the considered pump sources works at 800 nm (Ti:Saphire lasers), delivering pulses in the 50 - 1500 fs range, while the other works at 1030 nm (Yb-doped lasers), delivering pulses in the 200 - 1500 fs range. The damage threshold intensity of crystals is approximately proportional to $1/\sqrt{\tau_0}$ [22]. Therefore, the pump intensity was chosen according to

$$I_0 = I_0^*\sqrt{\frac{100\mathrm{fs}}{\tau_0}}, \tag{9}$$

where $I_0^* = 100\frac{\mathrm{GW}}{\mathrm{cm}^2}$ is the peak pump intensity at 100 fs. In this way, the used pump intensity is about four times lower than the damage threshold on the whole investigated pump pulse length range. By choosing relatively low pump intensity, many nonlinear effects become irrelevant.

4. Results

Figure 3 shows the optical-to THz conversion efficiency predicted for the RNLS source as a function of the pump pulse length and the crystal length for 800 and 1030 nm pump wavelengths. Maximal efficiency can be achieved at 4 mm crystal length and ~400 fs pump pulse length in the examined region.

According to our calculations, higher efficiency can be reached at 800 nm, than at 1030 nm. The reason for this is that the variation of the pump pulse length with the pump propagation is slower for shorter wavelengths, what results in longer interaction length [8]. However, the three

Optics EXPRESS

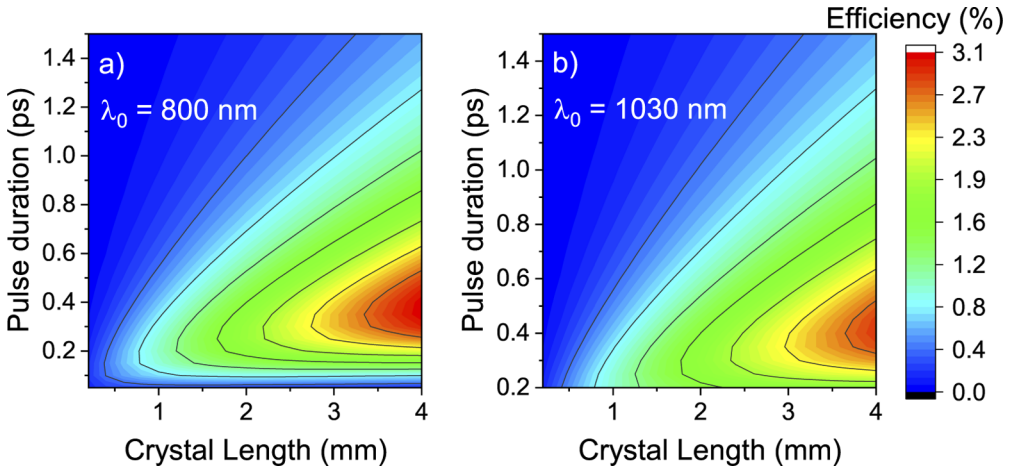

Fig. 3. Optical-to THz conversion efficiency as a function of the pump pulse length and the crystal length for 800 (a) and 1030 nm (b) pump wavelengths.

photon absorption can negatively influence the efficiency in the case of 800 nm pump laser, while it does not occur at 1030 nm [23]. This effect was not taken into account in our simulations. Since all the presented results except Fig. 2(a) and Fig. 3(a) were calculated for 1030 nm pump wavelength, three photon absorption does not influence our findings significantly.

As it is seen in Fig. 3, the optimal pump pulse length to reach maximal efficiency increases with the crystal length. For example, the optimal FL pump pulse length is 200 fs for 1 mm, but it is 400 fs for 4 mm crystal length at 1030 nm pump wavelength. Consequently, it is practical to use longer crystals if the FL pulse length of the available pump source is relatively long. For a given crystal length the efficiency increasing with decreasing FL pump pulse length. This is reasinable since according to Eq. (9) the pump peak intensity is larger for shorter FL pump pulse length. Hovewer, for very short FL pump pulse length the pump pulse duration changes very fast during propagation inside the NM resulting much longer average pulse duration than the FL one, and consequently a dropping of the efficiency.

It is worth to determine the temporal characteristics of the electric field strength, which are important for several applications, especially for particle acceleration. Figure 4 shows the THz pulseforms (Figs. 4(a) and 4(c)) and the corresponding spectra (Figs. 4(b) and 4(d)) for 2 (Figs. 4(a) and 4(b)) and 4 mm (Figs. 4(c) and 4(d)) crystal lengths at 1030 nm pump wavelength. The peak electric field strength is 575 kV/cm for a 2 mm crystal, while it is 700 kV/cm for 4 mm length. The spectral peak shifts towards lower frequencies as the crystal length gets longer, since the absorption coefficient of the LN increases with the THz frequency.

As it is seen in Fig. 4, the main THz cycle is followed by several oscillations for short FL pump pulses. The reason for this is the material dispersion of the LN in the THz range. This explanation is supported by Figs. 4(b) and 4(d). The THz spectrum becomes broader for shorter pump pulses. Due to the large spectral bandwidth, the material dispersion has significant influence on the temporal pulse shape, a chirp is introduced. THz absorption results in narrowing of the spectrum in long crystals (Fig. 4(d)). However, the effect of the dispersion remains significant because of the long propagation distance. Accordingly, it follows that the appearance of the oscillations can not be significantly influenced by the crystal length.

As it is evident from Fig. 4, THz pulses become perfectly single-cycle for FL pump pulse lengths longer than 1 ps. The central frequency of the THz pulse decreases with increasing pump pulse duration. For the sake of clarity, Fig. 5 shows a few selected pulse shapes with their corresponding spectra.

Optics EXPRESS

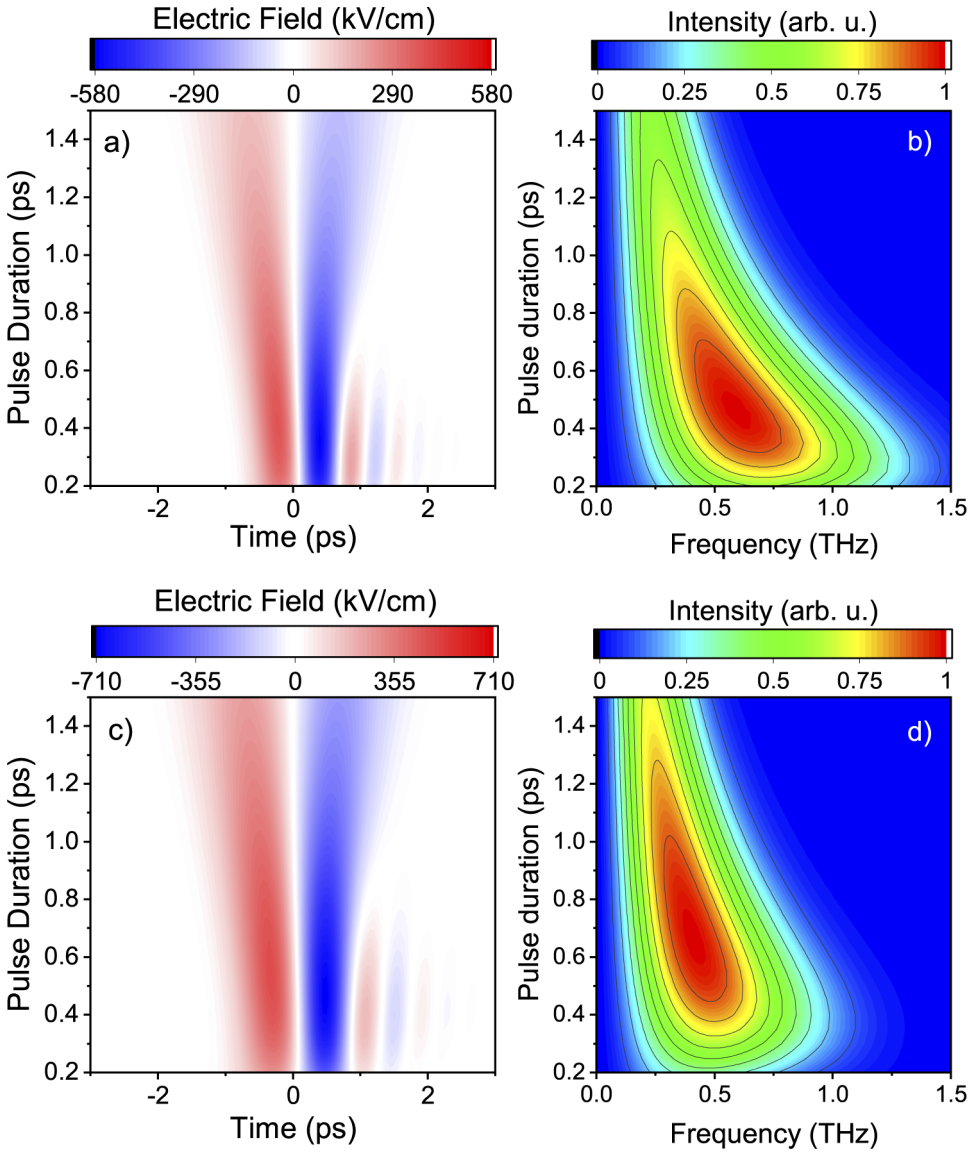

Fig. 4. THz pulseforms (a,c) and the corresponding spectra (b,d) for 2 (a,b) and 4 mm (c,d) crystal lengths.

Beside its simplicity, the other main important advantage of the RNLS source is that there is no principal limitation for its excitation surface. Consequently, there are no principle limitations for the scalability of the THz pulse energy. Extreme large electric field strength can be achieved by focusing THz pulses excited by RNLS having large surface. For the demonstration of this, we supposed pump pulses with 1 ps FL pulse length, 870 mJ energy, 7 cm beam diameter, 1030 nm wavelength and crystal length of 4 mm. According to Fig. 3, the optical-to-THz generation efficiency is 1.25 %, i.e. the THz pulse energy is 10.8 mJ in this case. ~50 MV/cm peak electric field strength can be obtained by focusing the generated 7 cm diameter THz beam with an off axis parabolic mirror of 5 cm effective focal length. Figure 6 shows the THz pulse shapes directly behind the RNLS and in the focus. Although the pulse shape becomes somewhat distorted by

Optics EXPRESS

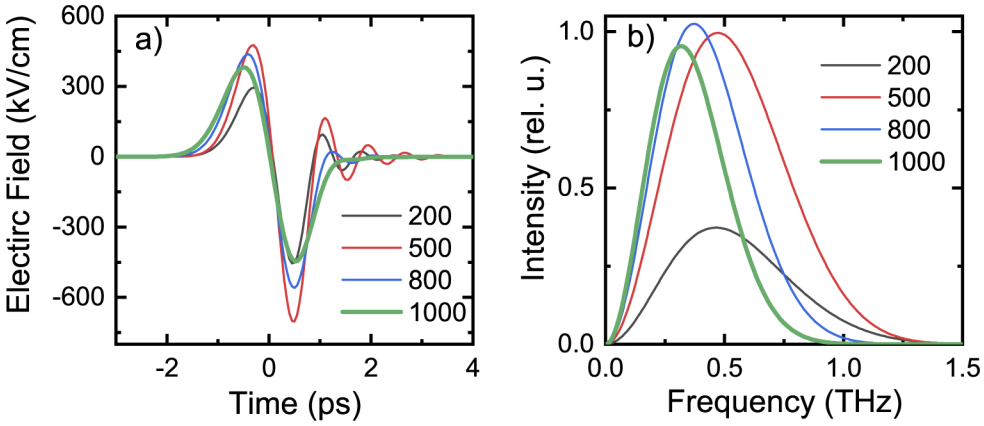

Fig. 5. THz pulseshapes (a) and the corresponding spectra (b) for several FL pump pulse lengts supposing 4 mm crystal length.

focusing [24,25], since the foci of the spectral components of the broad THz spectra are spatially separated, the focused field remains nearly single-cycled. This property makes this THz pulse extremely suitable for particle acceleration. Our results suggest that even longer than 4 mm crystal lengths may be applicable if the pump pulse length is over 1 ps.

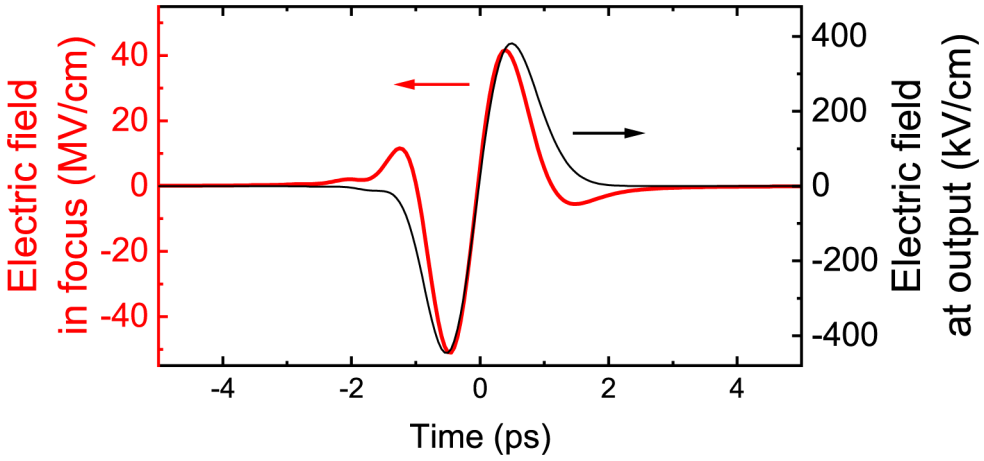

Fig. 6. Terahertz pulse shapes directly after exiting the RNLS (black) and after focusing (red) supposing 4 mm crystal length, 1 ps FL pump pulse length, 7 cm beam diameter, 5 cm focal length. The pulse energies of the pump and the THz are 870 and 10.8 mJ, respectively.

5. Discussion

The proposed RNLS TPF THz pulse source overcomes limitations (i) and (ii), namely the imaging errors, and the necessity of the use of the prism shaped NM. Although the angular dispersion (iii) is not reduced, for pump pulses longer than 200 fs the setup predicts good optical-to-THz generation efficiencies even for pump intensities well below the damage threshold, and for relatively short crystals.

As it was pointed out in the Introduction, the setup suggested by Ofori et al. [15] is free of angular dispersions, but is limited by the factors (i) and (ii). In order to reduce the effect of

Optics EXPRESS

angular dispersion in the above discussed RNLS arrangement, wich is absent of limiting factors (i) and (ii), we propose to use it in high diffraction order (e.g. m $\gg$ 50 at 30 fs FL pulse duration). This means that the d grating constant also has to be increased significantly, so practically the RNLS works as a ribbed reflector. Such a setup can be applied, if the time delay between the neighbouring zones is larger than the pump pulse length. According to our calculation (and in accordance with a recent study [26]), for 30 fs pump pulse duration approximately three times larger efficiency can be achieved by RNLS working in the 150^{th} order than working in the 20^{th} order.

The weakness of this solution is the destructive THz interference coming from the segmented pump pulse front. This can be overcome by a double structure, which is a combination of a rough and a fine structure as shown in Fig. 7. Similarly to the hybrid property of the NLES [16] the necessary average pulse front tilt is also created by both diffraction and reflection in this structure, but here the diffractive and reflective elements are integrated. The theoretical modeling and quantitative analysis of this altered RNLS structure are not the subject of the present paper, since deeper considerations are needed.

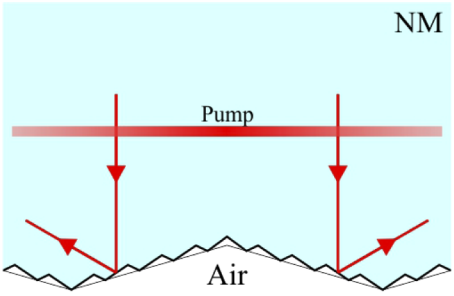

Fig. 7. Schematic of a double structure RNLS consisting of a rough and a fine structure.

All the previously discussed results belong to simulations at 300 K. We found that the efficiencies are nearly doubled at 100 K, due to the lower THz absorption of the LN. The optimal crystal length for obtaining single-cycle pulses is shorter for 100 K than for 300 K, while the optimal pump pulse length is larger for 100 K than for 300 K. This behavior of the parameters can be explained by the fact that the THz spectrum shifts towards higher frequencies due to the lower THz absorption at lower temperatures.

It is important to note, that simulated efficiency values exceeding 2% are not reliable, because of several limiting effects due to the presence of intense THz field as discussed in [27]. Such effects might be taken into account in a more complex model in the future. The goal of the present paper was to show the advantages of the proposed RNLS setup in the frame of a simple model. These advantages are the scalability of the THz pulse energy and the extremely large available peak electric field strength together with spatially uniform THz beam properties.

LN was used as NM in the above discussed simulations. However, the advantages of the RNLS setup can also be exploited using other NM, for example semiconductor.

6. Conclusion

We introduced an imaging free, slab shaped THz pulse source, which allows the upscaling of the THz pulse energy without principal limitations. The temporal characteristics of the electric field strength is uniform along the whole cross section of the THz beam independently of the beam spot size. Perfect single cycle pulses with efficiency exceeding 1% can be generated by FL pump pulses of 1 ps length. Several 10 - 100 MV/cm peak electric field strength can be achieved by the focusing, depending on the beam spot size. These properties open the way for several novel

Optics EXPRESS

applications of high energy THz pulses. For example, such pulses can play important role in the field of THz-based particle acceleration [1–4].

Funding

Emberi Eroforrások Minisztériuma (EFOP-3.6.1-16-2016-00004, EFOP-3.6.2-16-2017-00005); Nemzeti Kutatási Fejlesztési és Innovációs Hivatal (125808).

Acknowledgments

This paper was supported by the János Bolyai Research Scholarship of the Hungarian Academy of Science (Gy. T.); European Union, co-financed by the European Social Fund grant EFOP-3.6.1-16-2016-00004 entitled by Comprehensive Development for Implementing Smart Specialization Strategies at the University of Pécs and grant EFOP-3.6.2-16-2017-00005 entitled by Ultrafast physical processes in atoms, molecules, nanostructures and biological systems.

References

1. E. A. Nanni, K.-H. H. W. R. Huang, K. Ravi, A. Fallahi, G. Moriena, R. J. D. Miller, and F. X. Kärtner, "Terahertz-driven linear electron acceleration," Nat. Commun. **6**(1), 8486 (2015).
2. D.-F. Zhang, A. Fallahi, M. Hemmer, X.-J. Wu, M. Fakhari, Y. Hua, H. Cankaya, A.-L. Calendron, L. E. Zapata, N. H. Matlis, and F. X. Kärtner, "Segmented terahertz electron accelerator and manipulator (steam)," Nat. Photonics **12**(6), 336–342 (2018).
3. L. Pálfalvi, J. A. Fülöp, G. Tóth, and J. Hebling, "Evanescent-wave proton postaccelerator driven by intense thz pulse," Phys. Rev. Spec. Top.–Accel. Beams **17**(3), 031301 (2014).
4. A. Sharma, Z. Tibai, and J. Hebling, "Intense tera-hertz laser driven proton acceleration in plasmas," Phys. Plasmas **23**(6), 063111 (2016).
5. C. Vicario, A. V. Ovchinnikov, S. I. Ashitkov, M. B. Agranat, V. E. Fortov, and C. P. Hauri, "Generation of 0.9-mj thz pulses in dstms pumped by a cr:mg2sio4 laser," Opt. Lett. **39**(23), 6632–6635 (2014).
6. J. Hebling, G. Almási, I. Kozma, and J. Kuhl, "Velocity matching by pulse front tilting for large-area thz-pulse generation," Opt. Express **10**(21), 1161–1166 (2002).
7. J. A. Fülöp, Z. Ollmann, C. Lombosi, C. Skrobol, S. Klingebiel, L. Pálfalvi, F. Krausz, S. Karsch, and J. Hebling, "Efficient generation of thz pulses with 0.4 mj energy," Opt. Express **22**(17), 20155–20163 (2014).
8. J. A. Fülöp, L. Pálfalvi, G. Almási, and J. Hebling, "Design of high-energy terahertz sources based on optical rectification," Opt. Express **18**(12), 12311–12327 (2010).
9. M. Kunitski, M. Richter, M. D. Thomson, A. Vredenborg, J. Wu, T. Jahnke, M. Schöffler, H. Schmidt-Böcking, H. G. Roskos, and R. Dörner, "Optimization of single-cycle terahertz generation in linbo3 for sub-50 femtosecond pump pulses," Opt. Express **21**(6), 6826–6836 (2013).
10. J. Hebling, "Derivation of the pulse front tilt caused by angular dispersion," Opt. Quantum Electron. **28**(12), 1759–1763 (1996).
11. L. Pálfalvi, J. A. Fülöp, G. Almási, and J. Hebling, "Novel setups for extremely high power single-cycle terahertz pulse generation by optical rectification," Appl. Phys. Lett. **92**(17), 171107 (2008).
12. J. A. Fülöp, G. Polónyi, B. Monoszlai, G. Andriukaitis, T. Balciunas, A. Pugzlys, G. Arthur, A. Baltuska, and J. Hebling, "Highly efficient scalable monolithic semiconductor terahertz pulse source," Optica **3**(10), 1075–1078 (2016).
13. Z. Ollmann, J. Hebling, and G. Almási, "Design of a contact grating setup for mj-energy thz pulse generation by optical rectification," Appl. Phys. B: Lasers Opt. **108**(4), 821–826 (2012).
14. M. Tsubouchi, K. Nagashima, F. Yoshida, Y. Ochi, and M. Maruyama, "Contact grating device with fabry-perot resonator for effective terahertz light generation," Opt. Lett. **39**(18), 5439–5442 (2014).
15. B. K. Ofori-Okai, P. Sivarajah, W. R. Huang, and K. A. Nelson, "Thz generation using a reflective stair-step echelon," Opt. Express **24**(5), 5057–5068 (2016).
16. L. Pálfalvi, G. Tóth, L. Tokodi, Z. Márton, J. A. Fülöp, G. Almási, and J. Hebling, "Numerical investigation of a scalable setup for efficient terahertz generation using a segmented tilted-pulse-front excitation," Opt. Express **25**(24), 29560–29573 (2017).
17. P. S. Nugraha, G. Krizsán, C. Lombosi, L. Pálfalvi, G. Tóth, G. Almási, J. A. Fülöp, and J. Hebling, "Demonstration of a tilted-pulse-front pumped plane-parallel slab terahertz source," Opt. Lett. **44**(4), 1023–1026 (2019).
18. G. Tóth, L. Pálfalvi, J. A. Fülöp, G. Krizsán, N. H. Matlis, G. Almási, and J. Hebling, "Numerical investigation of imaging-free terahertz generation setup using segmented tilted-pulse-front excitation," Opt. Express **27**(5), 7762–7775 (2019).
19. D. Huo, Z. J. Choong, Y. Shi, J. Hedley, and Y. Zhao, "Diamond micro-milling of lithium niobate for sensing applications," J. Micromech. Microeng. **26**(9), 095005 (2016).

Optics EXPRESS

20. M. I. Bakunov and B. Bodrov, "Terahertz generation with tilted-front laser pulses in a contact-grating scheme," J. Opt. Soc. Am. B **31**(11), 2549–2557 (2014).
21. K. L. Vodopyanov, "Optical generation of narrow-band terahertz packets in periodically-inverted electro-optic crystals: conversion efficiency and optimal laser pulse format," Opt. Express **14**(6), 2263–2276 (2006).
22. B. C. Stuart, M. D. Feit, A. M. Rubenchik, B. W. Shore, and M. D. Perry, "Laser-induced damage in dielectrics," Phys. Rev. Lett. **74**(12), 2248–2251 (1995).
23. S.-C. Zhong, Z.-H. Zhai, J. Li, L.-G. Zhu, J. Li, K. Mend, Q. Liu, L.-H. Du, J.-H. Zhao, and Z.-R. Li, "Optimization of terahertz generation from $linbo_3$ under intense laser excitation with the effect of three-photon absorption," Opt. Express **23**(24), 31313–31323 (2015).
24. S. Hunsche, S. Feng, H. G. Winful, A. Leitenstorfer, M. C. Nuss, and E. P. Ippen, "Spatiotemporal focusing of single-cycle light pulses," J. Opt. Soc. Am. A **16**(8), 2025–2028 (1999).
25. S. Feng, H. G. Winful, and R. W. Hellwarth, "Gouy shift and temporal reshaping of focused single-cycle electromagnetic pulses," Opt. Lett. **23**(5), 385–387 (1998).
26. K. Ravi, B. K. Ofori-Okai, K. A. Nelson, and F. X. Kärtner, "Analysis of terahertz generation by beamlet superposition," (2018). https://arxiv.org/abs/1810.09118v2.
27. K. Ravi, W. R. Huang, S. Carbajo, X. Wu, and F. Kärtner, "Limitations to thz generation by optical rectification using tilted pulse fronts," Opt. Express **22**(17), 20239–20251 (2014).